

ULTRASONIC SCATTERER STRUCTURE CLASSIFICATION WITH THE GENERALIZED SPECTRUM

Kevin D. Donohue (Senior Member IEEE), and Lexun Huang

Department of Electrical Engineering, University of Kentucky, Lexington, KY 40506

ABSTRACT

Ultrasonic back-scattered echoes resulting from the structures within a scanned object contain information of potential diagnostic value. The most common nondestructive evaluation (NDE) techniques use large-scale changes in the back-scatterer coefficients to reveal boundaries between materials with different density/elasticity properties or defects in homogenous material regions. Less common techniques consider small-scale scatterer characteristics that give rise to textures and other features not readily seen in the A-scan envelope or intensity image. This paper considers applying the generalized spectrum (GS) for classifying small-scale scatterer structures into three broad categories, diffuse, specular, and regular. The GS distinguishes between stationary (diffuse scattering) and certain classes of nonstationary processes based on a statistical characterization of the phase spectrum, and the GS can be normalized to limit variations due to frequency selectivity of the scatterers and the ultrasonic propagation path. This paper explains how the GS can be applied to classify scatterer structures over small sections of the ultrasonic A-scan and demonstrates its classification performance with simulations. The significance of the approach to NDE applications, such as flaw detection in homogenous material and material characterization in more complex material, is also discussed.

1. INTRODUCTION

A pulse of ultrasonic energy can penetrate materials under inspection. The pulse structure results from the transducer and determines the maximum resolution achievable by the system. The interaction of the propagating pulse with the material inhomogeneities (scatterers) creates a back-scatterer signal consisting of unstructured energy from the diffuse (unresolvable) scatterers and structured energy from single isolated scatterers or quasi-periodic scatterers. Diffuse scatterer echoes produce a stationary random process from which material properties, such as frequency attenuation and frequency scatterer response, can be determined through the power spectral density (PSD) [1,2]. Specular and quasi-periodic scatterer echoes exhibit structure similar to that of the interrogating pulse. They also give rise to textures and boundaries important in creating an image to reveal internal structure and characteristics [2].

This paper describes a GS application for detecting signal regions of the A-scan that cannot be considered stationary [3]. In particular, simulation results illustrate the GS response to three types of A-scan scatterers: diffuse only, diffuse plus

specular, and diffuse plus quasi-periodic. A set of parameters related to the response of each scatterer type are extracted from the GS and used to detect the presence of nonstationary data created by the specular and quasi-periodic scatterers. Receiver operating characteristics (ROC) [4] demonstrate detection performance.

2. GS PARAMETERS

The GS characterizes the correlation between distinct frequency components. Let $y(t)$ denote the back-scattered echoes and $Y(f)$ its spectrum. The GS is defined [5] by:

$$GS(f_1, f_2) = E[Y(f_1)Y^*(f_2)] \quad (1)$$

where $E[\cdot]$ is the expected value operator and superscript $*$ indicates a complex conjugate. Note for $y(t)$ a stationary random process, the diagonal of the GS in the bifrequency plane ($f_1 = f_2$) is equivalent to the PSD. The off-diagonal values of the GS ($f_1 \neq f_2$) are complex and have the potential to characterize structure (regular phase patterns) in the data.

The key property enabling the GS application presented here is that for any wide-sense stationary process the value of the GS is zero for $f_1 \neq f_2$. Thus, through various normalization and averaging techniques [5,6], the GS function is estimated over a region of interest, and if the off-diagonal components values are close to zero, the region is declared to have diffused only scatterers. In this case characterizations for stationary random processes would be appropriate for this region. On the other hand, if significant deviations from zero are detected, the presence of specular or quasi-periodic scatterers is declared and the region is considered nonstationary.

If the signal-to-noise ratio is reasonably constant over the bandwidth of the system, the GS can be reduced to a one-dimensional function through a collapsed average (CA) [6]. The collapsed average takes advantage of phase coherence along the diagonals of the GS that occurs when either periodic or coherent echoes are present. Thus coherent averaging along the diagonals (where $f_1 = f_2 + \text{constant}$) allow for further suppression of diffuse echo contributions.

Figure 1 illustrates the CA response for three cases. The quasi-periodic and specular echoes were simulated with a 20 dB structured-to-diffuse echo power ratio. Each segment of the ultrasound scan was energy normalized [5,6] before time averaging the outer products of the DFT vector to estimate the GS. The collapsed average was computed by taking the magnitude of the coherent averages along each diagonal. The

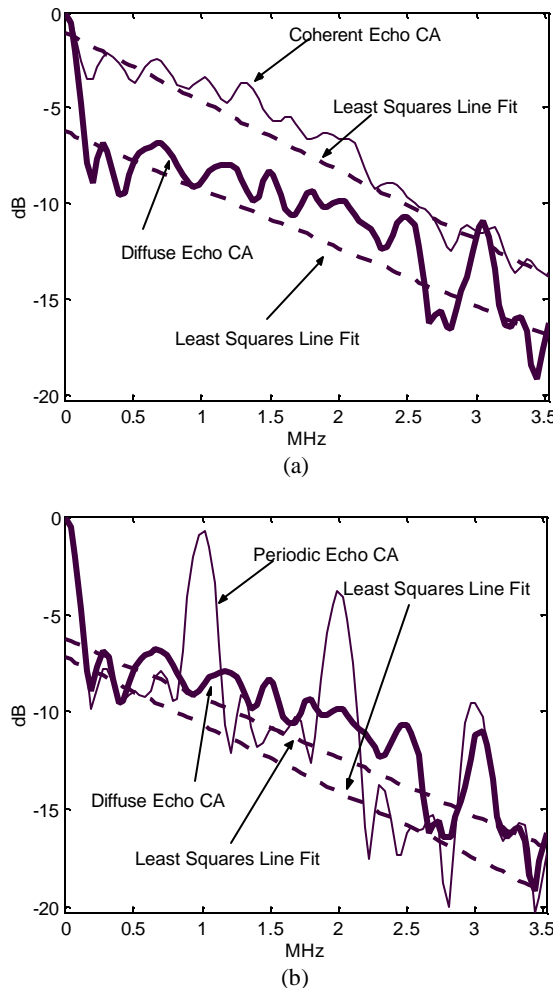


Fig. 1. Examples of the energy normalized CA with best line fit comparison of diffuse echo only with (a) coherent scatterers (b) periodic scatterers.

abscissa of the CA is the constant difference between f_1 and f_2 that corresponds to the diagonal averaged. The simulated pulse had a 3 MHz bandwidth over which the CA was computed.

Figure 1(a) contrasts the resulting phase coherence along each diagonal with that of the diffuse echoes. Note the 5 dB difference between the CA values over the pulse bandwidth. This distinction diminishes at the end and beginning of the axis shown, which corresponds to the limits of the useful system bandwidth. The high frequency limit of the CA corresponds to correlations at the end of the system bandwidth (i.e. resolution limit for smallest scatterer spacing). The low frequency end of the CA is mainly affected by length and shape of the time window (smallest resolvable frequency difference).

Figure 1(b) contrasts CA values between diffuse echoes and quasi-periodic echoes. Note that the periodic structures create coherence at frequency differences inversely proportional to the spacing in time. At frequency differences not corresponding to this spacing or its harmonics, the CA has a similar lack of coherence as the diffuse case. A line is fit to the censored log of

the CA to create a best line fit. A line is initially fit in a least-squares sense to the CA; and 50% of the points that most deviate in the positive direction from that line are censored out and the line is fit again to the remaining data for the final result. The censoring operation helps reduce the effects of the peaks due to regular spacing as observed in Fig. 1(b).

Figure 1 suggests several CA parameters useful for discriminating between regions containing different scatterer types. Table 1 presents an indexed list of the 12 different features. The area under the CA and the best line fit parameters are important CA features for discriminating between specular (highly coherent echoes) and diffuse echo regions [7]. These features provide a quantitative measure of the coherence of the echoes in a region of interest. Regions containing strong isolated scatterers or boundaries with sharp changes in density and elasticity yield high values for the area under the CA. Specular echoes also directly affect the slope and y-intercept values, with the y-intercept being more sensitive than the slope. The important CA features for detecting and estimating regularly spaced or periodic scatterers are the areas between the best line fit and the CA over various subbands along the frequency axis [6]. The CA curve is divided into sub-bands because different size structures correspond to different regions under the curve. The particular time interval regions along the CA axis used in this study are given by parameters 4 through 11 in Table 1. The CA peak at 1, 2, and 3 MHz in Fig. 1(b) correspond to the 1 μ s pulse spacing in time.

3. SIMULATION EXPERIMENTS

The performance of GS-based parameters to detect either specular or periodic scatterers embedded in diffuse scatterers is examined by computing the receiver operating characteristics (ROC) from simulated A-scans [6,7]. The ROC is a plot of the detection probability as a function of false alarm (i.e. deciding that a diffuse-only region contains a specular or periodic scatterer). The area under the resulting ROC curve is presented to assess the overall detection performance. An ROC area of 1 indicates a perfect separation between the classes, while an 0.5 ROC area corresponds to no separation between the classes.

For each scatterer class a Monte Carlo simulation was performed with 300 A-scans of a 32 μ s duration, which represented the region of interest. The GS parameters were computed using time averaging [8] with 3 μ s segments at a 50% overlap (corresponding to about 10 independent averages per region). The scatterers were modeled as a sequence of impulse functions with a random amplitude range from 0.1 to 0.9. The A-scan is formed by convolving the impulse sequence and the system response modeled by a modulated Rayleigh pulse:

$$h(t) = t \sin(2\pi f_c t) \exp\left(-t^2/2\sigma^2\right), \quad (2)$$

where f_c the center frequency is set to 7 MHz, and σ is directly proportional to the effective pulse width. The σ value was chosen in these simulations to set the effective pulse width to about 0.6 μ s. Scatterers within this interval are unresolvable.

A-scans with diffuse only, diffuse plus periodic, and diffuse plus specular scatterers were generated. The diffuse scatterer

Parameter Index	Description
1	Total area under CA curve
2	Slope of best-line fit
3	y-intercept of best-line fit
4	2.58-1.43 μ s regular structures area
5	1.43-0.99 μ s regular structures area
6	0.99-0.76 μ s regular structures area
7	0.76-0.61 μ s regular structures area
8	0.61-0.52 μ s regular structures area
9	0.52-0.44 μ s regular structures area
10	0.44-0.39 μ s regular structures area
11	0.39-0.35 μ s regular structures area
12	Maximum of parameters 4 -11

Table 1. List of CA parameters

scans contained about 17 scatterers per microseconds. The spacings for the periodic scatterers were generated with Gamma distributed random variables. The mean spacing was set to 2μ s with 3 cases of increasing spacing variance (5, 10, and 15 percent of the mean scatterer spacing). This resulted in about 2 scatterers per 3μ s segment, which was used in the time-averaging estimate of the GS. Specular scatterer A-scans were computed for 4 cases by randomly distributing 1, 2, 4, and 8 scatterers over the 32μ s scan. Since there are more 3μ s segments than scatterers, some segments in the region of interest contain diffuse-only A-scans. The scatterer density value is used to denote these 4 concentrations, which is given by the average number of specular scatterers occurring in any 3μ s segment. Two different diffuse scatterer power-to-coherent or periodic scatterer power ratios (SNR) were used. The power ratio between the diffuse and structural scatterers is set by scaling the structural scatterer waveform to obtain either 12dB or 0 dB for the 2 different SNR cases. A -30 dB additive white noise component was added to all scans.

Figure 2 presents the coherent scatterer detection performance for GS parameters 1 and 3. The scatter densities range from about 0.1 (i.e. on average 1 out of every 10 segments contain a specular scatterer) to 0.8 as shown in the abscissa of the plot. While both parameters indicate good performance for high densities and high SNR, the CA area shows more sensitivity (good performance at low density) and robustness (good performance at lower SNR) than all the other parameters including the y-intercept parameter, which is also shown. The CA area results from the maximum amount of averaging over the bifrequency plane of the GS. This parameter was also used in flaw detection in [7]. If the flaw is embedded in a sea of diffuse scatterers, and the flaw scatterer has one or two effective scattering centers, similar performance, as shown here, can be expected. Similar performance is observed between the energy normalized and system normalized GS with a better performance observed for the energy normalized GS.

Figure 3 presents the periodic scatterer detection performance for GS parameters 4-11 and 12, which are the most responsive to coherent scatterers. The 2μ s second spacing

forms peaks in the CA at frequency intervals of $1 / (2\mu$ s) = 0.5 MHz. The spacing area parameter is the average of all parameters from 4-11 that correspond to the 0.5 MHz harmonics. The maximum value parameter, on the other hand, is the maximum value of the parameters 4-11. The variance of the scatterer spacing is increased for two different SNR values. The plots show that at low scatterer spacing variance and high SNR, both parameters work well. As variance is increased, the spacing area parameter shows the most sensitivity, as well as more robustness to the noise power from the diffuse scatterers. This is expected because the spacing area parameters take advantage of additional statistical averaging over the information contained throughout the GS. The disadvantage of the spacing area is that the spacing has to be known beforehand or a set of averaging templates must be applied for all possible spacings (detection and spacing estimation would be done simultaneously in this case). A significant amount of work has been done to detect and estimate periodic scatterers [8,9]. In this simulation, since only two scatterers were present per segment, these results can be extended to the detection of spacing from duct and tube walls. This problem was looked at in greater detail in [6].

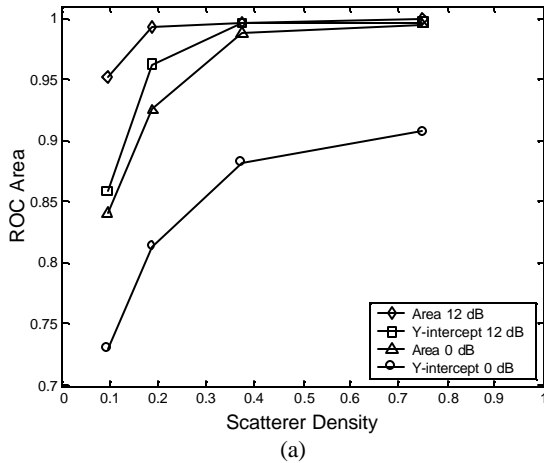
Similar performance results are observed for both the system normalized and energy normalized GS parameters. A minor performance loss is observed in both Figs. 2 and 3 for the system normalized GS. This is due to information from coherent and periodic scatterers that is also present in the magnitude spectra as well as the phase. However, in complex media with variable scatterer and material-path frequency responses, the magnitude spectra can be significantly affected by factors other than the scatterer type. Simulation and phantom studies typically show that the energy normalized GS performs better than the system normalized GS [6]. Studies using actual tissue for classification purposes indicate that the system normalized GS performs better [5].

4. CONCLUSIONS

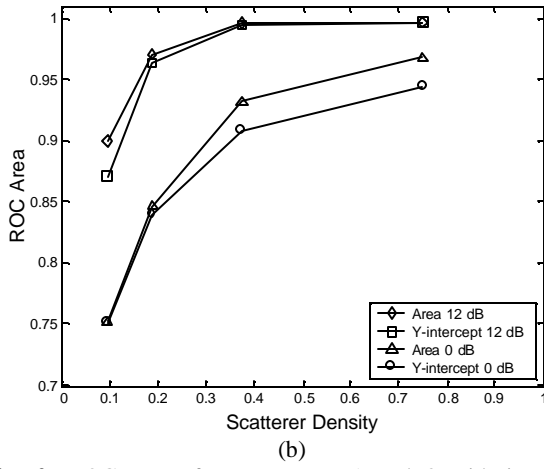
The automatic classification of regions of ultrasonic scatterers into diffuse (statistically stationary), specular, and periodic (nonstationary) scatterers allows proper methods to be applied for further analysis of the data. The GS provides a means for classifying A-scan segments in this way. Applications to flaw detection in homogenous material are analogous to detecting coherent or specular scatterers as described in this work. The area under the CA was shown to be the best parameter in this case. Complex scattering patterns generated by quasi-periodic scatterers give rise to textures in B-scan intensity images. These patterns also can be detected by the GS parameters by breaking the CA into subbands corresponding to spacing ranges and taking the area between the best line fit and the CA. The subband areas can be combined (weighted average) to match the expected pattern.

5. ACKNOWLEDGEMENTS

This work was supported in part by the National Cancer Institute and the National Institutes of Health Grant PO1-CA52823.

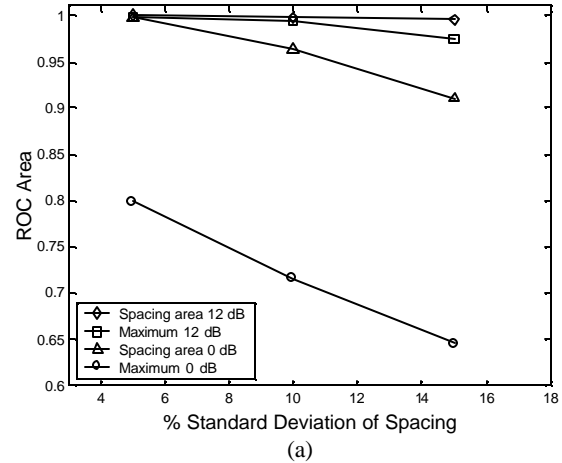


(a)

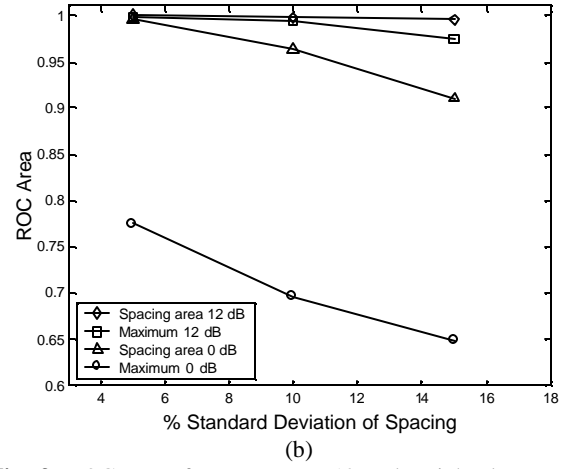


(b)

Fig. 2. ROC areas for parameters 1 and 3 with increasing number of coherent scatterers in region of interest. (a) For energy normalized CA (b) For system normalized CA.



(a)



(b)

Fig. 3. ROC areas for parameters 12 and weighted average of parameters 4 through 11 with increasing standard deviation of mean scatterer spacing. (a) For energy normalized CA (b) For system normalized CA.

6. REFERENCES

- [1] F.L. Lizzi, M. Ostromogilsky, E.J. Feleppa, et. al., Relationship of Ultrasonic spectral parameters to features of tissue microstructure, *IEEE Trans. Ultrason Ferroelect Freq Contr* vol. 34, pp. 319-328 1987.
- [2] R.F. Wagner, M.F. Insana, and D.G. Brown, and T. Hall, "Describing small-scale structure in random media using pulse-echo ultrasound," *J. Opt. Soc. of Am.*, vol. 4, pp. 910-922, May 1987.
- [3] N.L. Gerr and J.C. Allen, The generalized spectrum and spectral coherence of a harmonizable time series, *Digital Signal Processing*, vol. 4, pp. 222-238, 1994.
- [4] C.E. Metz, Some practical issues of experimental design and data analysis in radiological ROC studies, *Invest. Radiol.*, Vol. 24, 234-245, 1989.
- [5] K.D. Donohue, F. Forsberg, C.W. Piccoli, and B.B. Goldberg, "Analysis and Classification of Tissue with Scatterer Structure Templates," *IEEE Trans. Ultrason., Ferroelect., Freq. Contr.*, vol. 42, pp. 451-463, May 1995.
- [6] K.D. Donohue, L. Huang, V. Genis and F. Forsberg, Duct size detection and estimation in breast tissue, *Proceeding of 1999 IEEE Ultrasonics Symposium*, vol. 2, pp. 1353-1356, 1999.
- [7] "Spectral Correlation Filters for Flaw Detection," K.D. Donohue and H.Y. Cheah, *Ultrasonics Symposium*, pp. 725-728, 1995.
- [8] T. Varghese and K.D. Donohue, Mean-scatterer spacing estimates with spectral correlation, *J. Acoust. Soc. Am.* 96 (6), Dec. 1994.
- [9] T. Varghese and K.D. Donohue, Estimating mean scatterer spacing with the frequency-smoothed spectral autocorrelation function, *IEEE Trans. Ultrason., Ferroelect., Freq. Contr.*, vol. 42, pp. 451-463, May 1995.